Differentiation xxx (xxxx) xxx–xxx

Contents lists available at ScienceDirect

Differentiation

journal homepage: www.elsevier.com/locate/diff

Three-dimensional imaging of the developing human fetal urogenital-genital tract: Indifferent stage to male and female differentiation☆

Dylan Isaacson[a], Joel Shen[b], Maya Overland[b], Yi Li[b], Adriane Sinclair[b], Mei Cao[b], Dylan McCreedy[c], Meredith Calvert[c,d], Todd McDevitt[c], Gerald R. Cunha[b], Laurence Baskin[b,e,*]

[a] Department of Urology, Northwestern University Feinberg School of Medicine, Chicago, IL, USA
[b] Department of Urology, University of California, San Francisco, San Francisco, CA, USA
[c] J. David Gladstone Institutes, San Francisco, CA, USA
[d] Histology and Light Microscopy Core, J. David Gladstone Institutes, San Francisco, CA, USA
[e] Division of Pediatric Urology, University of California San Francisco Benioff Children's Hospital, 550 16th St, 5th Floor, Mission Hall Pediatric Urology, San Francisco, CA 94158, USA

ARTICLE INFO

Keywords:
Three-dimensional imaging
Scanning electron microscopy
Optical projection tomography
Lightsheet microscopy
Human fetal urogenita tract

ABSTRACT

Recent studies in our lab have utilized three imaging techniques to visualize the developing human fetal urogenital tract in three dimensions: optical projection tomography, scanning electron microscopy and lightsheet fluorescence microscopy. We have applied these technologies to examine changes in morphology and differential gene expression in developing human external genital specimens from the ambisexual stage (< 9 weeks fetal age) to well-differentiated male and female organs (> 13 weeks fetal age). This work outlines the history and function of each of these three imaging modalities, our methods to prepare specimens for each and the novel findings we have produced thus far. We believe the images in this paper of human fetal urogenital organs produced using lightsheet fluorescence microscopy are the first published to date.

1. Introduction and background

An understanding of complex phenomena in the development of the urogenital system requires visualization of developing structures in three dimensions. Recent studies, enabled by the novel application of three-dimensional (3D) imaging modalities, have elucidated mechanisms of development of the urethra in the human penile shaft and of analogous structures in the clitoris (Li et al., 2015; Overland et al., 2016; Shen et al., 2016). 3D imaging has revealed that development of the human urogenital tract is more intricate and complex than previously appreciated. This work will outline three key techniques we have applied to the study of the development of the human fetal urogenital tract, describe the novel findings that have resulted from each and discuss future applications of these modalities to the field.

1.1. History of three-dimensional reconstruction

The use of 3D reconstruction has been instrumental in the study of development since the late 19th century (Hopwood, 1999). In 1876, Gustav Born first described his method of hand-tracing enlarged projections of microtome-sectioned embryos onto wax plates, allowing embryologists to create scaled models of structures of interest via serially stacking the plates, physically cutting out the relevant structures and melting them together (Born, 1883). This method, applied by Franklin Mall and other anatomists at the Johns Hopkins University in the late 19th and early 20th centuries, helped enable morphologic studies that still form much of the basis of our understanding of human development in the embryonic period (Fig. 1) (Mall, 1891). In the century since the time of Born and Mall, newer, automated modalities of 3D reconstruction have continued to add to our knowledge of how

Abbreviations: 3D, Three-dimensional; BABB, Benzyl alcohol/benzyl benzoate; DBE, Dibenzyl ether; FISH, Fluorescent in situ hybridization; K6, Cytokeratin 6; K7, Cytokeratin 7; LSFM, Lightsheet fluorescence microscopy; NA, Numerical aperture; OPT, Optical projection tomography; PACT, PAssive Clarity Technique; PCR, Polymerase chain reaction; PFA, Paraformaldehyde; RIMS, Refractory index matching solution; SDS, Sodium dodecyl sulfate; SEM, Scanning electron microscopy; SRY, Sex determining Y region; UCSF, University of California, San Francisco

☆ Supported by NIH grant K12DK083021.

* Corresponding author at: University of California San Francisco Benioff Children's Hospitals, Department of Urology, 550 16th St, 5th Floor, Mission Hall Pediatric Urology, San Francisco, CA 94158, USA.
E-mail address: Laurence.baskin@ucsf.edu (L. Baskin).

https://doi.org/10.1016/j.diff.2018.09.003
Received 1 August 2018; Received in revised form 30 August 2018; Accepted 3 September 2018

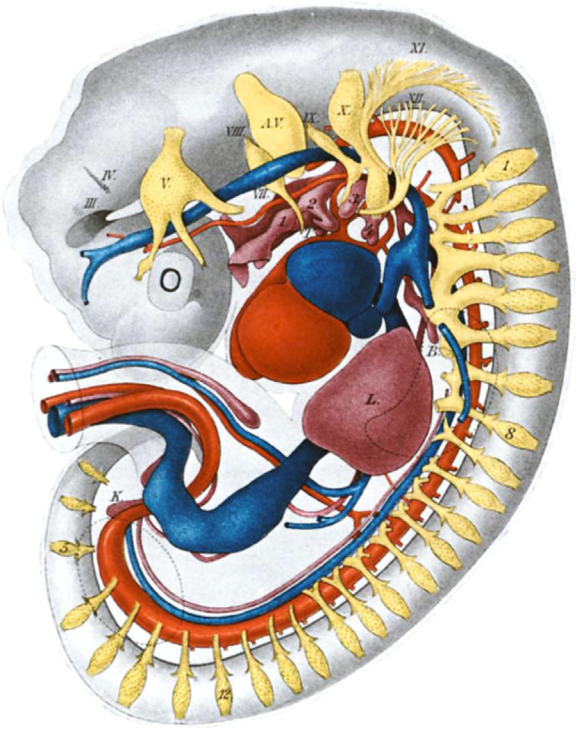

Fig. 1. [26-day old human embryo wax plate] reconstruction viewed from the left side. Enlarged 15 times. HI., IV., V., etc. cranial nerves; A.V., auditory vesicle; I. 2, 3, and 4, branchial pockets; T. thyroid gland; B. bronchus; L. liver; K. kidney; yellow, nerves; red, arteries; blue, veins. The dotted lines mark the extremities. Reproduced from Mall FP. A human embryo twenty-six days old. (1891) Journal of Morphology 5: 459–480. Public domain.

human urogenital organs form in a less labor-intensive fashion, however many of the basic principles of reconstruction remain the same.

1.2. Optical projection tomography (OPT)

OPT is a newer technique, designed and first described by James Sharpe in 2002 (Sharpe et al., 2002). Its invention conferred the ability to assess specimen morphology and gene expression patterns in intact specimens larger than 1 mm, the limit of imaging depth for two-photon confocal microscopes (Sharpe, 2004). Projection tomography refers to 3D reconstruction of an object from multiple two-dimensional "projections": the images detected after electromagnetic radiation is passed through an entire specimen from varying angles (Fig. 2). As proportions of structures in the projections change with the angle of the applied radiation, a mathematical transformation must be applied to reconstruct the object in three dimensions (Sharpe et al., 2002). In the case of OPT, the wavelength of the electromagnetic radiation is in the visible spectrum, allowing for selective excitation of fluorophore-conjugated antibodies or fluorescent in situ hybridization (FISH) probes. This enables 3D localization of nucleic acids or products of gene expression in their native locations. OPT's imaging depth of up to 1 cm makes it ideal for imaging many relatively large human embryonic and fetal urogenital organs. Of note, OPT requires that light be able to pass through imaged specimens without scattering or diffraction, so specimens must be rendered optically transparent via equilibration in organic solvents such as benzyl alcohol/benzyl benzoate (BABB) or dibenzyl ether (DBE) in addition to fluorescent staining (Richardson and Lichtman, 2015).

1.3. Scanning electron microscopy (SEM)

Modern scanning electron microscopes operate based on many of the same principles originally outlined by Manfred von Ardenne in 1937 (McMullan, 1995). Electron microscopes consist of an electron

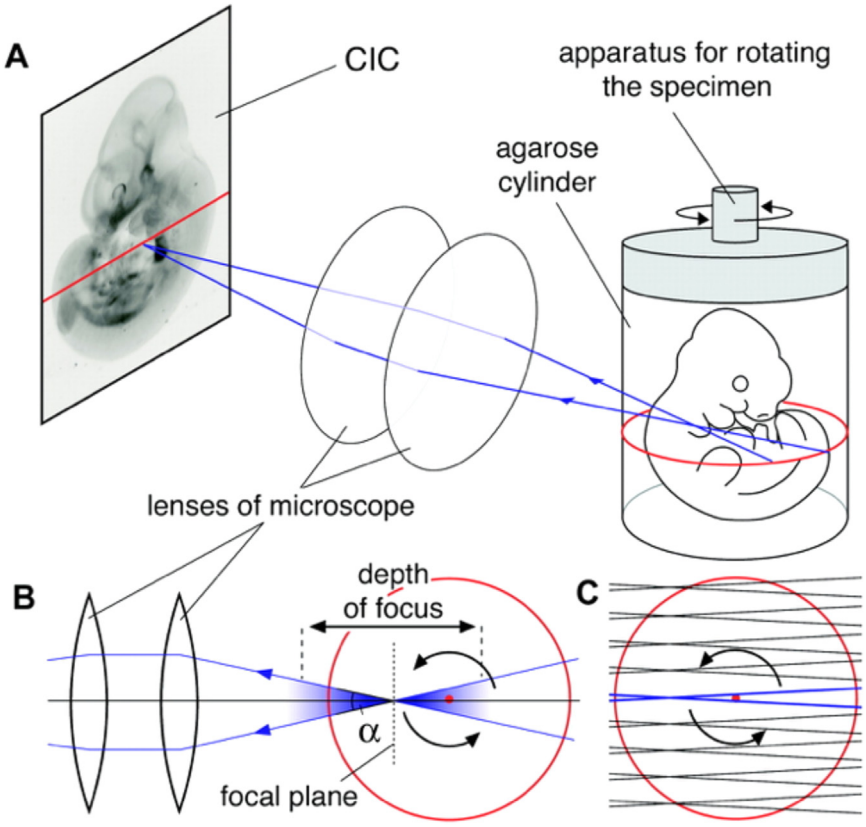

Fig. 2. OPT microscopy. (A) A schematic of the OPT microscopy setup. The specimen is rotated within a cylinder of agarose while held in position for imaging by a microscope. Light transmitted from the specimen (blue lines) is focused by the lenses onto the camera-imaging chip (CIC). The apparatus is adjusted so that light emitted from a section that is perpendicular to the axis of rotation (red ellipse) is focused onto a single row of pixels on the CIC (red line). The section highlighted as a red ellipse in (A) is seen as a red circle in (B). The region of the specimen sampled by a single pixel of the CIC is shown as a double inverted cone shape (blue region). Points far from the focal plane will not appear sharply focused in the image (pale blue shading), while those closer to the plane will be more focused (darker blue shading). (C) The sampled regions from adjacent pixels were distributed across the section as an approximation of parallel line integrals. Reproduced from Sharpe, J., U. Ahlgren, P. Perry, et al., Optical projection tomography as a tool for 3D microscopy and gene expression studies. Science, 2002. 296(5567): p. 541–5, with permission.

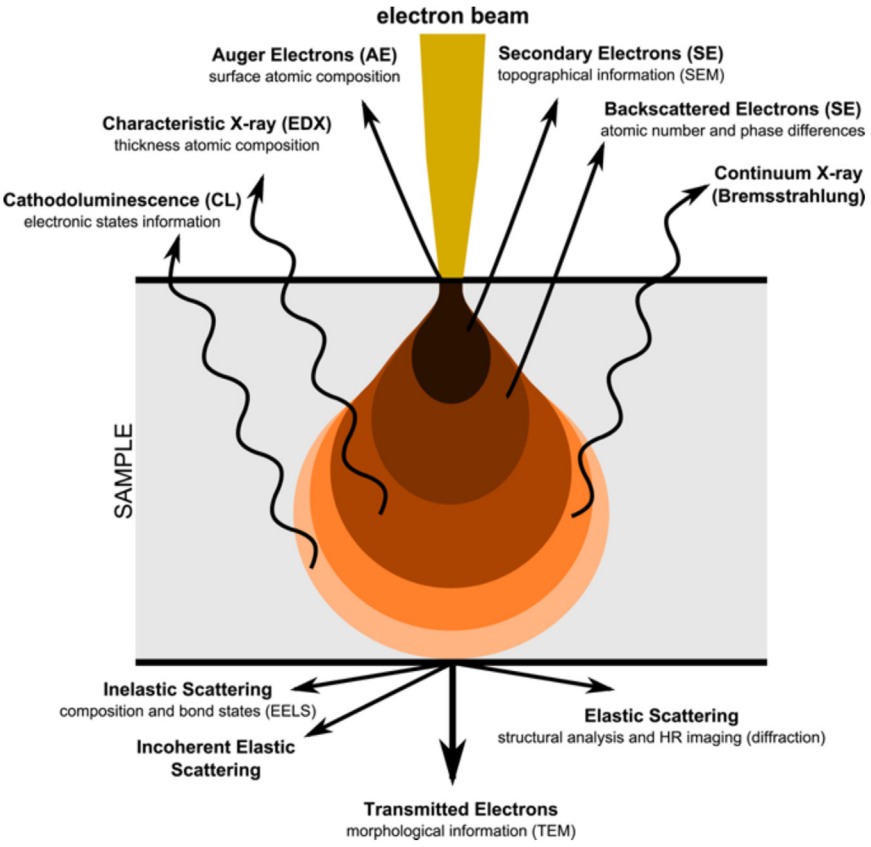

Fig. 3. Schematic of electron-sample interactions in electron microscopy. Each interaction produces multiple electron and electromagnetic signals, the detection of which gives different types of information about the sample. In scanning electron microscopy, low-energy secondary electrons excited from the sample are detected, providing topographical information that can be reconstructed into a 3D image as the electron beam is scanned across the sample. Image by Claudionico~commonswiki CC BY-SA 4.0, Created: 17 December 2013.

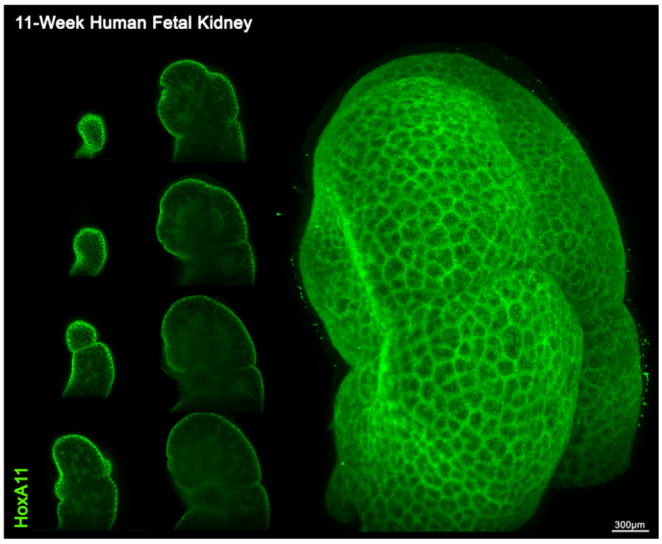

Fig. 4. 11-week human fetal kidney stained for metanephric mesenchyme-expressed HoxA11 and imaged using lightsheet fluorescence microscopy. Individual optical sections (left) are reconstructed into a full 3D representation (right). Each illuminated point directly corresponds to one voxel in the 3D reconstruction without the use of computerized transformation.

source which directs a stream of electrons through a series of apertures and lenses to create a highly focused beam of "primary" electrons with a spot size of about 5–10 nm. Excited "secondary" electrons originating from the surface of the specimen are detected by an overlying sensor, with the intensity of the detected signal varying with the topography and composition of the specimen (Fig. 3). The beam of electrons is mechanically scanned along the surface of the specimen, with the detected signal reconstituted into a full, magnified representation.

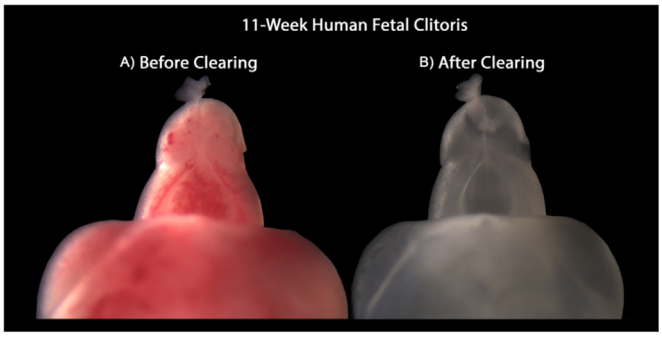

Fig. 5. 11-week human fetal clitoris before (A) and after (B) clearing with the PAssive Clarity Technique (PACT). Proteins and nucleic acids are stabilized in an acrylamide-based hydrogel matrix, allowing for lipids to be gently dissolved in sodium dodecyl sulfate (SDS) to attain specimen transparency while preserving molecular targets for whole-mount immunostaining.

(Reichelt, 2007). SEM is highly suited for analysis of the surface morphology of fetal urogenital organs in that it confers both high resolution and a depth of focus about 100x greater than conventional light microscopes, allowing for entire specimens to remain in focus throughout imaging. Despite its excellent resolution, SEM lacks the ability to visualize internal structures and identify fluorescently-labeled substances, making it most useful for studies describing external morphological changes through developmental time.

1.4. Lightsheet fluorescence microscopy (LSFM)

The concept of optical microscopy using thin sheets of visible light is not a new one. In 1903, the researchers Henry Sidentopf and Richard Zsigmondy at Carl Zeiss AG described the ultramicroscope, which used bright sunlight projected through a thin slit aperture to illuminate small

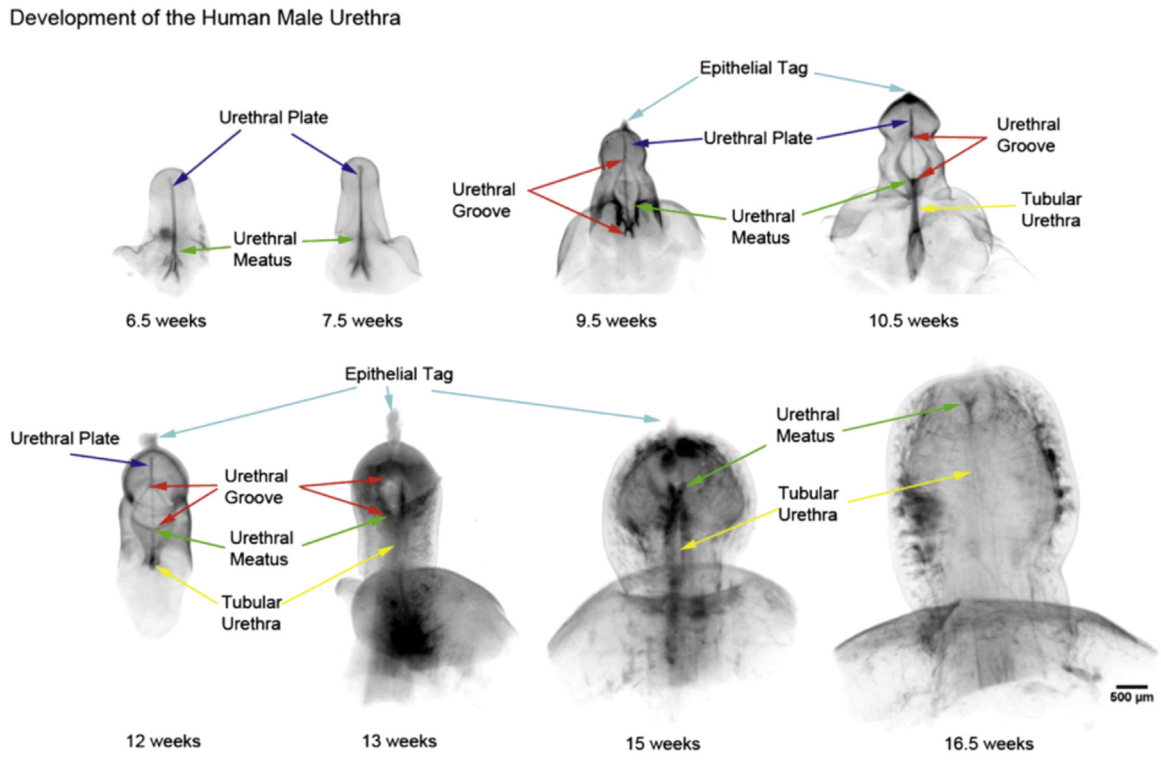

Fig. 6. Optical projection tomography of male urethral development from 6.5 to 16.5 weeks fetal age. Note the progression of the urethral meatus (green arrows) from the level of the scrotal folds at 6.5 weeks to its terminal position at the glans penis at 16.5 weeks. Wide open urethral groove (red arrows) is best seen from 9.5 to 13 weeks with clear progression of proximal to distal fusion of the edges of the urethral groove to form the tubular urethra (yellow arrows). At 13 weeks the urethral groove has reached the glans penis with the tubular urethra completely formed within the shaft of the penis. Reproduced from Li, Y., A. Sinclair, M. Cao, et al., Canalization of the urethral plate precedes fusion of the urethral folds during male penile urethral development: the double zipper hypothesis. J Urol, 2015. 193(4): p. 1353–59, with permission.

gold molecules in colloidal suspension (Siedentopf and Zsigmondy, 1903). Despite this early innovation, planar sheets of light were not applied to section fluorescently-labeled biologic specimens until 1993 (Voie et al., 1993). Subsequent developments in the field culminated in the release of the first commercial LSFM device by Zeiss, the Lightsheet Z.1, in 2012. LSFM has quickly grown in popularity due to its superior resolution to OPT and confocal microscopy, ability to image to a specimen depth of 1 cm, rapid speed of data acquisition and minimal phototoxicity allowing for imaging of live specimens over time.

LSFM operates based on section tomography as opposed to projection tomography as in OPT: in section tomography, each point in the specimen can be mapped onto 3D space without the need for the mathematical transformations used in projection tomography (Sharpe et al., 2002). LSFM devices achieve this via the application of a thin plane of light laterally to the sample and perpendicular to the plane of the recording objective. This “lightsheet” excites biomolecules only in that plane, minimizing extraneous background fluorescence (Fig. 4). The specimen is physically translated within the microscope as the lightsheet is quickly flickered on and off, resulting in a stack of optical sections that are used to reconstitute the full model (Stelzer, 2015). Once the model is reconstructed in 3D, colocalization and morphometric analyses can be digitally performed. Structural LSFM imaging can be performed using the autofluorescence of naturally occurring NADH, FAD and other biomolecules (Andersson et al., 1998). However, LSFM is usually utilized with exogenous fluorescent immunolabels, allowing for identification of products of gene expression in their native locations (Isaacson et al., 2017, 2018). Modern LSFM devices are able to selectively excite fluorophores of multiple wavelengths, allowing for double, triple and quadruple fluorescent stains in a single specimen. As in OPT, high quality fluorescent imaging requires optical clearing. Depending on the design of the LSFM device, this can be accomplished with equilibration of specimens in organic solvents, polylols or via lipid extraction methods such as the PAssive Clarity Technique (PACT) (Treweek et al., 2015).

2. Materials and methods

2.1. Specimen acquisition

Human fetal urogenital specimens were collected following elective termination procedures with approval from the institutional review board at the University of California, San Francisco (UCSF). At each gestational age 3-4 specimens were evaulated . The collection technique has been described in depth in prior publications (Cunha et al., 2016). Specimen age is estimated using heel-toe length (Drey et al., 2005), and sex is determined by polymerase chain reaction (PCR) of the sex-determining Y region (SRY) gene, morphology of Wolffian and Mullerian structures and/or the presence of testes and ovaries. *The accuracy of estimating gestational age is described in detail in the companion publication in this issue* (Shen et al., 2018a).

2.2. Optical projection tomography

Our group applied the OPT preparation protocol outlined by Sharpe et al. (2002): specimens were fixed in 10% neutral buffered formalin overnight, bleached with hydrogen peroxide, immersed in primary and secondary antibodies, optically cleared in BABB and embedded in agarose. Specimens were imaged with a 3001 M OPT scanner (Bioptonics, Edinburgh, Scotland). 400–800 projected images from each of two optical channels were transformed into 3-dimensional voxel datasets with in-house software. Datasets were visualized and measured in the Volocity software suite (PerkinElmer, Waltham, MA, USA).

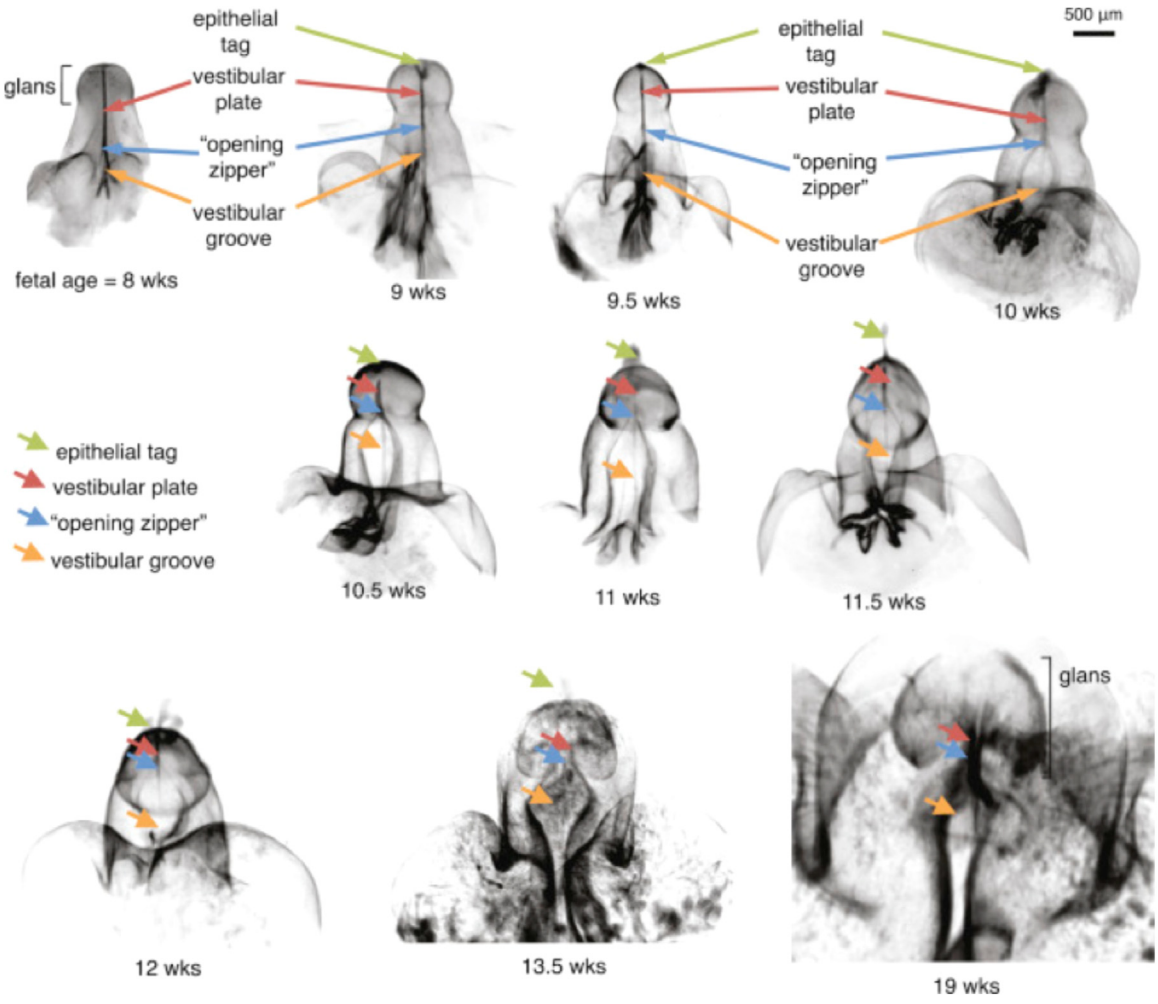

Fig. 7. Optical projection tomography of clitoral development from 8 to 19 weeks fetal age. Note the progression of distal canalization of the vestibular plate (red arrow) to form the wide open vestibular groove (orange arrow) by 13.5 weeks. Proximal fusion of the vestibular folds is absent throughout development. Reproduced from Overland, M., Y. Li, M. Cao, et al., Canalization of the Vestibular Plate in the Absence of Urethral Fusion Characterizes Development of the Human Clitoris: The Single Zipper Hypothesis. J Urol, 2016. 195(4 Pt 2): p. 1275–83, with permission.

2.3. Scanning electron microscopy

We prepare specimens for SEM as previously described (Shen et al., 2016). Specimens were fixed in 2% glutaraldehyde/0.1 M sodium cacodylate then post-fixed in 1% osmium tetroxide/0.1 M sodium cacodylate with intervening cacodylate washes. Following serial dehydration in ethanol, specimens were taken through critical point drying, mounted and imaged on a TM-1000 tabletop scanning electron microscope (Hitachi Ltd., Tokyo, Japan).

2.4. Lightsheet fluorescence microscopy

Specimens intended for LSFM were fixed in 4% paraformaldehyde (PFA) for 2–3 h at room temperature and stored in sterile PBS at 4 °C to allow for batched clearing and immunostaining. We cleared specimens using PACT (Fig. 5) (Treweek et al., 2015): Fixed organs were transferred to a 4 °C solution of 4% acrylamide in PBS supplemented with 0.25% thermoinitiator (VA-044, Wako Chemicals USA Inc., Richmond, VA) for 24 h. Oxygen was removed from the solution via bubbling 99.998% nitrogen gas for 1–5 min. Specimens were incubated in a 37 °C incubator for 2–3 h to initiate free-radical-induced acrylamide polymerization and stabilize biomolecules in the resultant hydrogel matrix.

Hydrogel-bound organs were immersed in 8% sodium dodecyl sulfate (SDS) in PBS and incubated at 37 °C with gentle agitation for 2–14 days until transparent (Fig. 5). Cleared specimens were submerged in blocking buffer (Super Block, Thermo Fisher Scientific, Waltham, MA, USA) for 24 h then immersed in up to three species-specific primary and secondary antibodies with intervening washes in PBS supplemented with 0.1% tween. Immunostained specimens were embedded in low-melting point agarose (Sigma-Aldrich, St. Louis, MO, USA) and allowed to equilibrate for at least 24 h in Histodenz (Sigma-Aldrich, St. Louis, MO, USA) refractory-index matching solution (RIMS) with refractive index of n = 1.46.

Human fetal urogenital organs were imaged using a 5x numerical aperture (NA) 0.16 detection objective lens on a Lightsheet Z.1 device (Carl Zeiss AG, Oberkochen, Germany) using Zeiss's ZEN Microscope Software. Z-stack output was reconstructed into three-dimensional datasets in Imaris (Bitplane AG, Zurich, Switzerland). Screenshots, point-to-point measurements and videos were recorded. Following imaging, the low melting point agarose was melted in a heating block set to 65 °C. Specimens were extracted and cleared of antibody via re-immersion in 8% SDS for 24–72 h, re-stained and re-imaged using the above protocol.

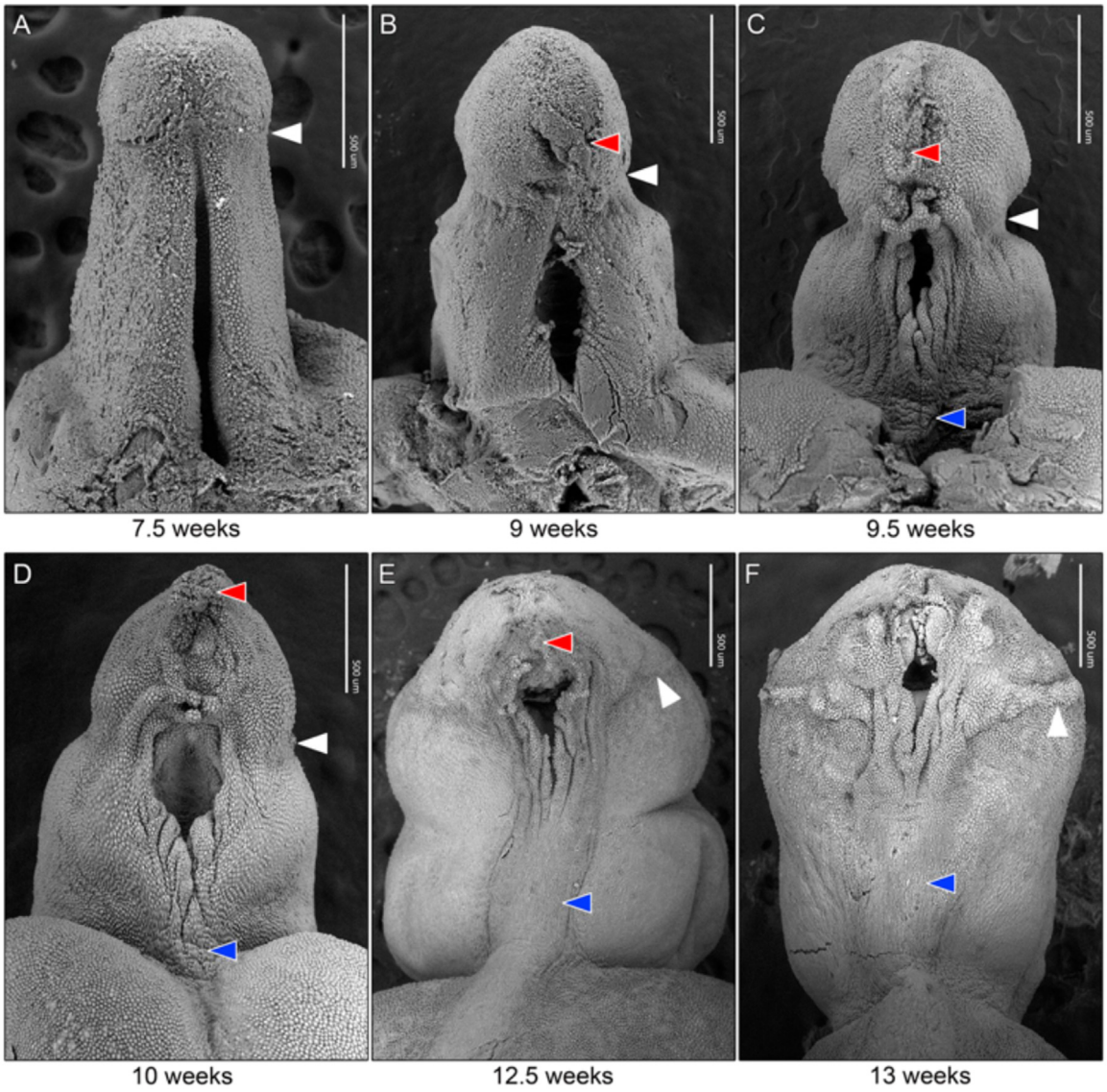

Fig. 8. Scanning electron microscopy ontogeny of the developing human fetal penis from 7.5 weeks to 13 weeks of gestation in ventral view. White arrowheads indicate the junction of the penile shaft to glans, red arrowheads indicate the distal epithelial tag, and blue arrowheads indicate the median penile raphe. Reproduced from Shen, J., M. Overland, A. Sinclair, et al., Complex epithelial remodeling underlie the fusion event in early fetal development of the human penile urethra. Differentiation, 2016. 92(4): p. 169–182, with permission.

3. Results

3.1. Optical projection tomography

Figs. 6 and 7 depict OPT images of human fetal penes and clitorides cleared and immunostained for the adherens junction component E-cadherin, which is expressed at epithelial surfaces (Gumbiner, 2005). The ages of the imaged external genital specimens ranged from the ambisexual stage of development (< 9 weeks fetal age) to well-differentiated fetal organs (> 16 weeks).

During male development (Fig. 6), a solid E-cadherin-labeled urethral plate was observed in the genital tubercle at the ambisexual stage (6.5, 7.5 weeks). The urethral plate canalized starting proximally and proceeding distally from 7.5 to 13 weeks, forming a wide-open urethral groove (Baskin et al., 2018). The urethral groove subsequently closed proximally to distally via fusion of the urethral folds, forming the mature tubularized urethra in the penile shaft (13 weeks). The epithelial tag at the distal tip of the glans penis was clearly visible in the 9.5–15-week specimens (Liu et al., 2018b).

In the female ontogeny (Fig. 7), a solid vestibular plate, the female homologue of the urethral plate, expressing E-cadherin was observed during the ambisexual stage (8 weeks) at a site analogous to that of the male urethral plate Overland et al., 2016). Proximal to distal canalization of the vestibular plate to form the vestibular groove was observed from 8 to 13 weeks. However, at no point was vestibular plate canalization observed in the glans clitoris nor did proximal fusion occur to close the vestibular groove. This pattern of development culminated in the well-differentiated morphology of the clitoris observed in the 19-week specimen. As in the male, the epithelial tag was present in the 9–13.5-week specimens.

3.2. Scanning electron microscopy

Figs. 8 and 9 depict SEM ontogenies of male and female human fetal external genitalia from the ambisexual stage to differentiated organs at 13 weeks. While internal structures such as the urethral plate are not visible on SEM, the surface morphology of the specimen and external features such as the epithelial tag are appreciable at a much higher

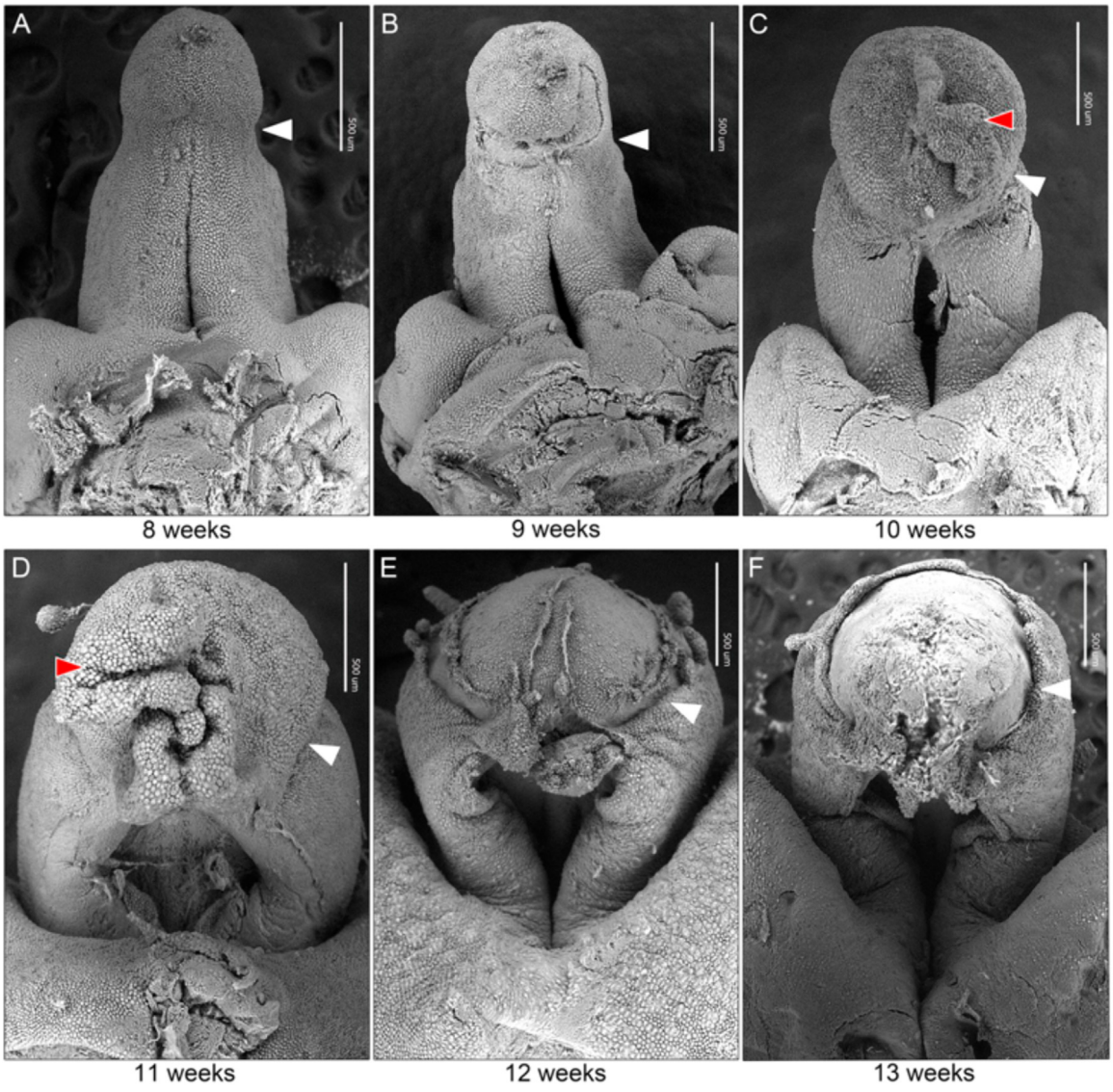

Fig. 9. Scanning electron microscopy ontogeny of the developing human fetal clitoris from 8 weeks to 13 weeks of gestation in ventral view. White arrowheads indicate the transition from clitoral shaft to glans; red arrowheads indicate the distal epithelial tag. Reproduced from Shen, J., M. Overland, A. Sinclair, et al., Complex epithelial remodeling underlie the fusion event in early fetal development of the human penile urethra. Differentiation, 2016. 92(4): p. 169–182, with permission.

resolution than that of OPT.

In the SEM ontogeny of male external genitalia (Fig. 8), both the proximal to distal canalization and fusion processes are readily identified between 8 and 13 weeks, corroborating the results observed in the OPT specimens (Shen et al., 2016). The urethral fold fusion process, however, was revealed to be more complex than a simple union between two epithelial surfaces. Rather, it consists of a sequential, multilayered, interlacing processes between ventral epidermal “cords”. Some of these cords are covered in balls of bulbous epithelial cells which may be in the process of sloughing. Formation of the median raphe of the penis was observed proximal to the interlacing epidermal cords, which did not fuse immediately, but maintained physical separation throughout much of the fusion process (Liu et al., 2018b).

In the ontogeny of the female external genitalia (Fig. 9), SEM revealed the proximal to distal canalization of the vestibular plate between 8 and 13 weeks and the absence of vestibular fold fusion, substantiating the observations made using OPT. No epithelial cording was observed at any point in the developmental series of the clitoris. The development of the vestibular folds which form the future labia minora and the partial closure of the vaginal vestibule proximally were both apparent with increasing fetal age.

3.3. Lightsheet fluorescence microscopy

Fig. 10 illustrates the canalization and fusion processes in analogous 11-week male and female human fetal external genitalia. These organs were successfully double-stained for cytokeratin 6 (K6, blue) which is expressed in the urethral plate and epidermal surfaces, and cytokeratin 7 (K7, red), which stains urothelium and the dorsal aspect of the vestibular groove (Southgate et al., 1999; Shen et al., 2018a). In the male specimen (Fig. 10A), the circumference and depth of the urethral groove were evident. Sites of distal canalization and proximal fusion were visible at a higher resolution than in comparable specimens in the OPT series, along with surface features such as the midline raphe that were not observed with OPT. The female specimen (Fig. 10B) also demonstrated distal canalization to form the K7-expressing open vestibular groove. Layering of K7 apical to K6 in the dorsal vestibular groove is visible as were superficial structures such as the epithelial tag (Shen et al., 2018b).

Fig. 11 demonstrates growth and development of the penile urethra

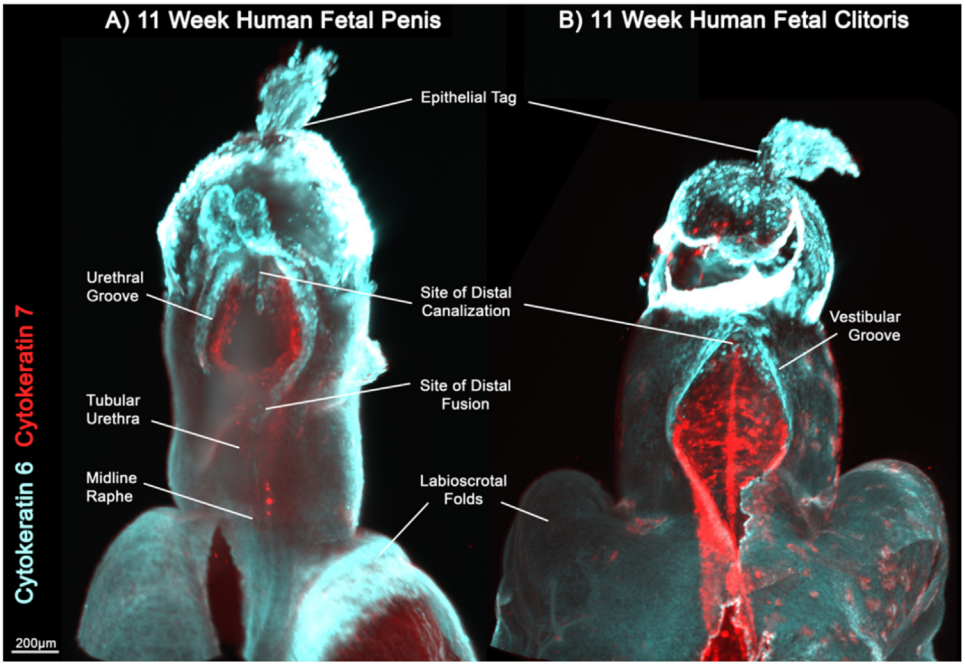

Fig. 10. Lightsheet fluorescence microscopy images of 11-week human fetal penis (A) and clitoris (B). Cytokeratin 6 (blue) is expressed in the urethral plate and epidermis and Cytokeratin 7 (red) is expressed in urothelium and the dorsal aspect of the vestibular groove. Proximal to distal canalization of the male urethral plate and the female vestibular plate has produced an open urethral groove in the penis and an open vestibular groove in the clitoris. Proximal to distal fusion of the urethral folds has produced the tubular urethral in the shaft of the male specimen only. In the clitoris, fusion does not occur, resulting in the mature open vestibular groove. Note the epithelial tag on both specimens.

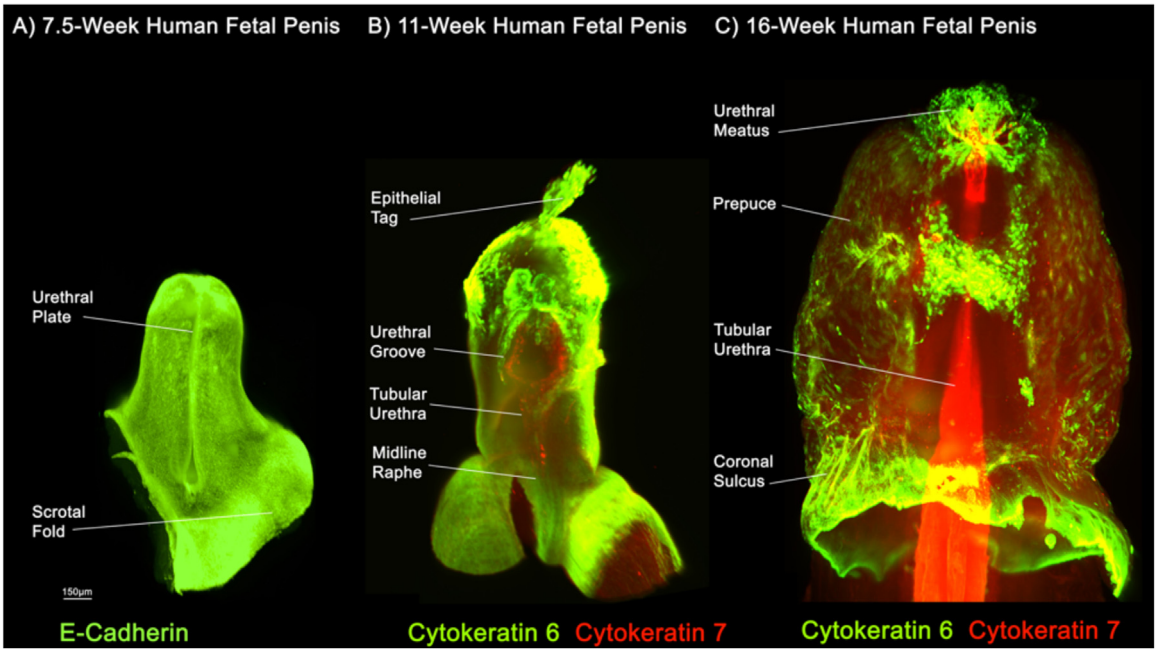

Fig. 11. Lightsheet fluorescence microscopy images demonstrating development of the penile urethra at the ambisexual stage (A, 7.5 weeks), during active urethral canalization and fusion to form the urethra in the penile shaft (B, 11 weeks) and during direct canalization to form the mature urethra in the glans penis (C, 16 weeks). E-cadherin is expressed at epithelial surfaces in development, Cytokeratin 6 is expressed in the urethral plate and epidermis and Cytokeratin 7 is expressed in urothelium.

from the ambisexual stage (7.5 weeks) to the point of distal canalization of the urethral plate in the glans (16 weeks) (Baskin et al., 2018; Liu et al., 2018b). The urethral plate, an internal structure, was clearly identified in the 7.5-week genital tubercle stained with E-cadherin (Fig. 11A) as in the OPT series. K6 (green)/K7 (red) double stains again illustrated progression of the urethral urothelium distally in relation to superficial epidermal structures. In contrast to the canalization/fusion processes seen in the 11-week specimen (Fig. 11B), the 16-week specimen (Fig. 11C) demonstrated a fully-formed K7-expressing tubular urethra proximally and a glandular urethral distally that is in the process of canalizing directly to form the urethral meatus distally. The K6-expressing prepuce is visible overlying the glans. An advantage of using LSFM is that the digital intensity of each fluorophore can be independently manipulated to optimally portray structures of interest. Applying this technique, the K6 signal was diminished in Fig. 11C to optimally reveal the K7 signal.

Fig. 12 shows the developing vasculature of analogous 11-week male and 10-week female fetal specimens. The male specimen (Fig. 12A) has extensive vasculature in the region of proximal uretheral fold fusion with vessel density greatest along the nascent midline raphe, which has been confirmed by standard immunostaining of tissue sections (unpublished results). The glans penis demonstrates tortuous

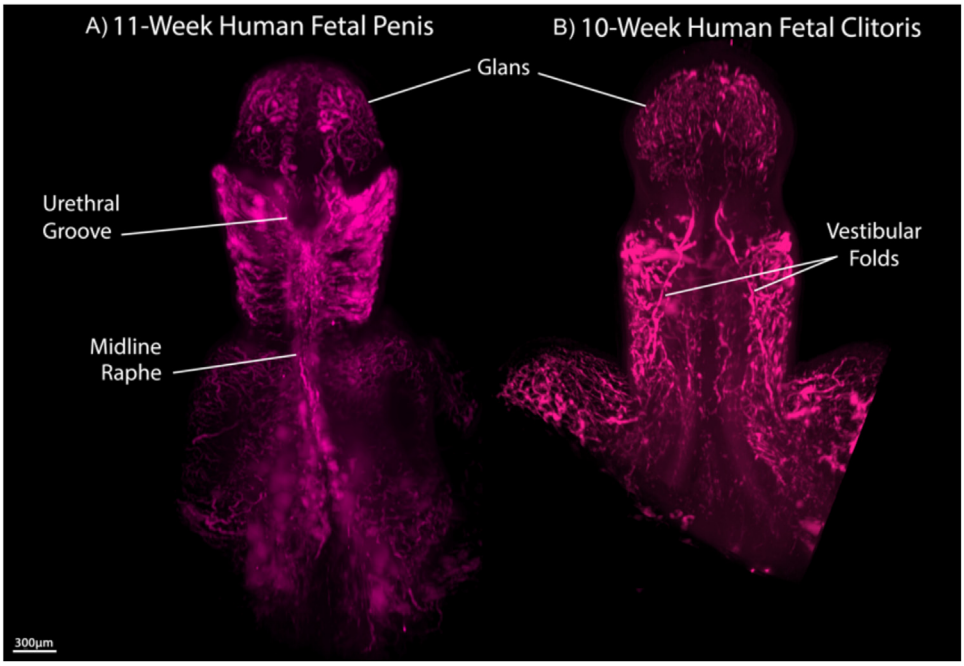

Fig. 12. Lightsheet fluorescence microscopy images of 11-week human fetal penis (A) and 10-week human fetal clitoris (B) demonstrating nascent vasculature. Note the dense regions of vasculature on the ventral surface around the canalizing urethral groove and fused midline raphe of the penis. This observation has been confirmed by standard immunostaining of tissue sections (unpublished observations) The clitoris demonstrates dense vascularity around analogous regions of the clitoral shaft with large vessels running along the medial aspects of the vestibular folds.

vessels except in the region of the urethral plate and distal urethral groove, in which vasculature is notably absent, consistent with different morphogenic mechanisms of urethral development proximally (urethral fold fusion) versus distally (direct canalization of the urethral plate) (Liu et al., 2018a). The female specimen (Fig. 12B) also demonstrated vascular density along the vestibular folds and clitoral shaft analogous to that seen in the 11-week penis. As in the male, the glans clitoris had extensive vasculature except in the region of the vestibular plate and distal vestibular groove.

4. Discussion

Herein we present 3D imaging techniques applied by our laboratory to investigate human penile and clitoral development in the late embryonic and fetal periods (Li et al., 2015; Overland et al., 2016; Shen et al., 2016). These methods have revealed new morphologic findings that have evaded detection through years of examination of serial histologic sections. Our use of OPT first allowed us to evaluate deep internal structures in intact, whole-mount immunostained penile and clitoral specimens. This led to our novel observations of the distal, E-Cadherin-labeled urethral plate opening to form the urethral groove and the groove closing to form the urethra within the penile shaft and midline raphe. Likewise, the nanometer resolution of SEM allowed us to characterize the ventral epidermal cords that constitute the proximal urethral fusion process, an unexpected result not seen in the fusion of other developing surfaces such as the palate (Waterman and Meller, 1974).

We believe that this work represents the first report of LSFM applied to image human fetal external genitalia. LSFM has largely supplanted OPT in our lab due to its superior resolution, the ability to re-stain and re-image specimens multiple times and its rapid speed of data acquisition. A full stack of LSFM optical sections can be acquired in about two minutes whereas it was previously necessary to leave an OPT specimen in the device overnight to produce a single model. This has enabled us to batch-process specimens and image up to ten specimens in a single LSFM microscopy session. We are working towards assembling full fetal urogenital organ ontogenies that can be immunostained and rapidly imaged before being cleared of antibody, re-stained for other antigenic targets and re-imaged. The novel application of LSFM has already resulted in our first whole-mount, double-stained images of K7-expressing urethral urothelium in the canalizing urethral groove and in the glandular urethra (Fig. 11). *A more extensive discussion of male and female external genitalia development can be found in two companion papers in this supplement* (Liu et al., 2018b; Baskin et al., 2018).

These prior discoveries open new frontiers in external genital development that our group and others are equipped to pursue: (a) The ventral cording that constitutes the proximal fusion process at the urethral groove should be investigated at the genetic and molecular level. The application of 20x magnification LSFM objective lenses should enable the whole-mount evaluation of fluorescently-labeled ventral cords, characterizing the signals governing this process. (b) The formation of the urethra in the human glans penis after 13 weeks fetal age has been poorly characterized. Three-dimensional evaluation of this process could be a major step in our understanding of the many cases of “standard” hypospadias in which the urethral meatus opens at the glans or coronal margin (Baskin, 2017). (c) We recently introduced our renal subcapsular xenografting method for evaluation of human urethral development (Isaacson et al., 2017) Evaluation of the morphogenesis of urethral and vestibular structures in xenografts and quantification of changes in expression of the androgen receptor in response to exogenous hormones should be conducted using 3D imaging. (d) Finally, the low levels of energy to which specimens are exposed in lightsheet microscopy enable non-invasive imaging of live organisms or tissues (Fei et al., 2016). *Ex vivo* tissue and organ culture methods are well-established in developmental biology (McClelland and Bowles, 2016). The Lightsheet Z.1 device has chambers equipped for specimen incubation and gas exchange. This should enable high-resolution imaging and analysis of developing murine and human external genital organs over time in varied transgenic lines and culture environments.

5. Conclusions

We have outlined the function and application of 3D imaging techniques to the study of human urogenital development. Scanning electron microscopy is most readily suited to the study of external features at extremely high resolution. Optical projection tomography and lightsheet fluorescent microscopy enable whole-mount evaluation of internal structures within cleared, fluorescently labeled specimens. Together these techniques have increased our understanding of the development of human penile urethral and clitoral structures in the late

embryonic and fetal periods. Novel applications of these technologies should enable further series of investigation into genetic control of urethral development, hormonal influences and the causes of hypospadias.

Funding sources

This work was supported by the National Institutes of Health [R01 DK058105/DK/NIDDK (LB), K12 DK083021/DK/NIDDK (AS)]; The American Urological Association/Urology Care Foundation Herbert Brendler, MD Research Fellowship (DI); The Alpha Omega Alpha Honor Medical Society Carolyn L. Kuckein Medical Student Research Fellowship (DI); and a Pathways to Discovery Project Grant from the University of California, San Francisco (DI).

References

Andersson, H., Baechi, T., Hoechl, M., Richter, C., 1998. Autofluorescence of living cells. J. Microsc. 191, 1–7.
Baskin, L., 2017. What is hypospadias? Clin. Pediatr. 56, 409–418.
Baskin, L., Shen, J., Sinclair, A., Cao, M., Liu, X., Liu, G., Isaacson, D., Overland, M., Li, Y., Cunha, J., 2018. Development of the human penis and clitoris. Differentiation (in this issue).
Born, G., 1883. Die Platten model lirmethode. Arch. Für Mikrosk. Anat. 22, 584–599.
Cunha, G., Overland, M., Li, Y., Cao, M., Shen, J., Sinclair, A., Baskin, L., 2016. Methods for studying human organogenesis. Differ.; Res. Biol. Divers. 91, 10–14.
Drey, E.A., Kang, M.S., McFarland, W., Darney, P.D., 2005. Improving the accuracy of fetal foot length to confirm gestational duration. Obstet. Gynecol. 105, 773–778.
Fei, P., Lee, J., Packard, R.R., Sereti, K.I., Xu, H., Ma, J., Ding, Y., Kang, H., Chen, H., Sung, K., Kulkarni, R., Ardehali, R., Kuo, C.C., Xu, X., Ho, C.M., Hsiai, T.K., 2016. Cardiac light-sheet fluorescent microscopy for multi-scale and rapid imaging of architecture and function. Sci. Rep. 6, 22489.
Gumbiner, B.M., 2005. Regulation of cadherin-mediated adhesion in morphogenesis. Nat. Rev. Mol. Cell Biol. 6, 622–634.
Hopwood, N., 1999. "Giving body" to embryos. Modeling, mechanism, and the microtome in late nineteenth-century anatomy. Isis; Int. Rev. devoted the Hist. Sci. Cult. Influ. 90, 462–496.
Isaacson, D., Shen, J., McCreedy, D., Calvert, M., Cunha, G., Baskin, L., 2017. Dichotomous branching of human fetal lung demonstrated with light sheet fluorescence microscopy. Am. J. Respir. Crit. care Med. 196, 1476–1477.
Isaacson, D., Shen, J., Cao, M., Sinclair, A., Yue, X., Cunha, G., Baskin, L., 2017. Renal subcapsular xenografting of the human fetal genital tissue- A new model for investigating urethral development. Differentiation 98, 1–13.
Isaacson, D., Shen, J., McCreedy, D., Calvert, M., McDevitt, T., Cunha, G., Baskin, L., 2018. Lightsheet fluorescence microscopy of branching human fetal kidney. Kidney Int 93, 525.
Li, Y., Sinclair, A., Cao, M., Shen, J., Choudhry, S., Botta, S., Cunha, G., Baskin, L., 2015. Canalization of the urethral plate precedes fusion of the urethral folds during male penile urethral development: the double zipper hypothesis. J. Urol. 193, 1353–1359.
Liu, G., Liu, X., Shen, J., Sinclair, A., Baskin, L., Cunha, G.R., 2018a. Contrasting mechanisms of penile urethral formation in mouse and human. Differentiation 101, 46–64.
Liu, X., Liu, G., Shen, J., Isaacson, D., Sinclair, A., Cao, M., Liaw, A., Cunha, G.R., Baskin, L.S., 2018b. Human glans and preputial development. Differentiation (in this issue).
Mall, F., 1891. A human embryo twenty-six days old. J. Morphol. 5 (3), 59.
McClelland, K.S., Bowles, J., 2016. Culturing murine embryonic organs: pros, cons, tips and tricks. Differ.; Res. Biol. Divers. 91, 50–56.
McMullan, D., 1995. Scanning electron microscopy 1928–1965. Scanning 17 (3), 175–185.
Overland, M., Li, Y., Cao, M., Shen, J., Yue, X., Botta, S., Sinclair, A., Cunha, G., Baskin, L., 2016. Canalization of the vestibular plate in the absence of urethral fusion characterizes development of the human clitoris: the single zipper hypothesis. J. Urol. 195, 1275–1283.
Reichelt, R., 2007. Scanning electron microscopy. In: Hawkes, P.W., S.J.C.H. (Ed.), Science of Microscopy. Springer, New York, NY.
Richardson, D.S., Lichtman, J.W., 2015. Clarifying tissue clearing. Cell 162, 246–257.
Sharpe, J., 2004. Optical projection tomography. Annu. Rev. Biomed. Eng. 6, 209–228.
Sharpe, J., Ahlgren, U., Perry, P., Hill, B., Ross, A., Hecksher-Sorensen, J., Baldock, R., Davidson, D., 2002. Optical projection tomography as a tool for 3D microscopy and gene expression studies. Science 296, 541–545.
Shen, J., Cunha, G., Sinclair, A., Cao, M., Isaacson, D., Baskin, L., 2018a. Macroscopic whole-mounts of the developing human fetal urogenital-genital tract: indifferent stage to male and female differentiation. Differentiation (in this issue).
Shen, J., Cunha, G.R., Sinclair, A., Cao, M., Liu, G., Isaacson, D., Baskin, L., 2018b. Immuohistochemical expression analysis of the human fetal lower urogenital tract. Differentiation (in this issue).
Shen, J., Overland, M., Sinclair, A., Cao, M., Yue, X., Cunha, G., Baskin, L., 2016. Complex epithelial remodeling underlie the fusion event in early fetal development of the human penile urethra. Differentiation 92, 169–182.
Siedentopf, H., Zsigmondy, R., 1903. Über sichtbarmachung und groessenbestimmung ultramikroskopischer teilchen, mit besonderer anwendung auf goldrubinglaesern. Ann. der Phys. 10, 1–39.
Southgate, J., Harnden, P., Trejdosiewicz, L.K., 1999. Cytokeratin expression patterns in normal and malignant urothelium: a review of the biological and diagnostic implications. Histol. Histopathol. 14, 657–664.
Stelzer, E.H., 2015. Light-sheet fluorescence microscopy for quantitative biology. Nat. Methods 12, 23–26.
Treweek, J.B., Chan, K.Y., Flytzanis, N.C., Yang, B., Deverman, B.E., Greenbaum, A., Lignell, A., Xiao, C., Cai, L., Ladinsky, M.S., Bjorkman, P.J., Fowlkes, C.C., Gradinaru, V., 2015. Whole-body tissue stabilization and selective extractions via tissue-hydrogel hybrids for high-resolution intact circuit mapping and phenotyping. Nat. Protoc. 10, 1860–1896.
Voie, A.H., Burns, D.H., Spelman, F.A., 1993. Orthogonal-plane fluorescence optical sectioning: three-dimensional imaging of macroscopic biological specimens. J. Microsc. 170, 229–236.
Waterman, R.E., Meller, S.M., 1974. Alterations in the epithelial surface of human palatal shelves prior to and during fusion: a scanning electron microscopic study. Anat. Rec. 180, 111–135.